

1 Evaluation of tropospheric SO₂ retrieved from MAX-DOAS 2 measurements in Xianghe, China

3
4 T. Wang^{1,2}, F. Hendrick², P. Wang¹, G. Tang¹, K. Clémer^{2,*}, H. Yu², C. Fayt², C.
5 Hermans², C. Gielen², G. Pinardi², N. Theys², H. Brenot², and M. Van Roozendael²

6 [1] Institute of Atmospheric Physics, Chinese Academy of Sciences, Beijing, China

7 [2] Belgian Institute for Space Aeronomy, Brussels, Belgium

8 *Now at: Instituut voor Sterrenkunde, Katholieke Universiteit Leuven, Leuven, Belgium

9 Correspondence to: Francois Hendrick (franch@oma.be)

10 11 Abstract

12 Ground-based Multi-Axis Differential Optical Absorption Spectroscopy (MAX-DOAS)
13 measurements of sulfur dioxide (SO₂) have been performed at the Xianghe station (39.8°N,
14 117.0°E) located at ~50 km southeast of Beijing from March 2010 to February 2013.
15 Tropospheric SO₂ vertical profiles and corresponding vertical column densities (VCDs),
16 retrieved by applying the Optimal Estimation Method to the MAX-DOAS observations, have
17 been used to study the seasonal and diurnal cycles of SO₂, in combination to correlative
18 measurements from in situ instruments, as well as meteorological data. A marked seasonality
19 was observed in both SO₂ VCD and surface concentration, with a maximum in winter
20 (February) and a minimum in summer (July). This can be explained by the larger emissions in
21 winter due to the domestic heating and, in case of surface concentration, by more favorable
22 meteorological conditions for the accumulation of SO₂ close to the ground during this period.
23 Wind speed and direction are also found to be two key factors in controlling the level of the
24 SO₂-related pollution at Xianghe. In the case of east or southwest wind, the SO₂ concentration
25 does not change significantly with the wind speed, since the city of Tangshan and heavy

1 polluting industries are located to the east and southwest of the station, respectively. In
2 contrast, when wind comes from other directions, the stronger the wind, the less SO₂ is
3 observed due to a more effective dispersion. Regarding the diurnal cycle, the SO₂ amount is
4 larger in the early morning and late evening and lower at noon, in line with the diurnal
5 variation of pollutant emissions and atmospheric stability. A strong correlation with
6 correlation coefficients between 0.6 and 0.9 is also found between SO₂ and aerosols in winter,
7 suggesting that anthropogenic SO₂ plays a more dominant role in the aerosol formation
8 compared to other sources during this season. The observed diurnal cycles of MAX-DOAS
9 SO₂ surface concentration are also in very good agreement (correlation coefficient close to 0.9)
10 with those from collocated in-situ data, indicating the good reliability and robustness of our
11 retrieval.

12 **1 Introduction**

13 Sulfur dioxide (SO₂), one of the most common air pollutants, is of major concern in pollution
14 control acts (Gauderman et al., 2000). In China, the Ministry of Environmental Protection
15 (MEP) lists SO₂ as one of the three conventional pollutants, together with NO₂ and PM₁₀, and
16 daily averaged SO₂ concentrations were used as an indicator to quantify the level of pollution
17 (Yan et al., 2010). This trace gas is predominantly produced by the burning of fossil fuels
18 including oil and coal, and the smelting of mineral ores that contain sulfur (Yan et al., 2005;
19 Zhao et al., 2012). SO₂ contributes to a large extent to the process of acidification resulting in
20 acid rain and to the formation of sulfate aerosols, both of which cause human health damages,
21 building surface corrosion, and visibility reduction. In particular, the secondary pollutant
22 sulfate aerosols generated by SO₂ are the primary source of fine solid particles in cities, which
23 are also responsible for severe air pollution issues (Meng et al., 2009). In addition, the
24 on-going industrial development, population growth, and heavy traffic contribute to higher
25 energy consumption and therefore, to an increase in SO₂ emissions into the atmosphere (Wu
26 et al., 2013). Consequently, in order to meet the urgent demand to improve and control air
27 quality in China, as well as to promote sustainable development, it is of the greatest

1 importance to study the evolution of a pollutant like SO_2 and to identify its possible origins.

2 So far, the SO_2 surface concentration has been monitored using in-situ and long-path DOAS
3 (Differential Optical Absorption Spectroscopy) instruments (Meng et al., 2009), while satellite
4 sensors like GOME, SCIAMACHY, GOME-2, OMI, OMPS, and IASI have shown their
5 ability to measure the SO_2 vertical column density (VCD) over polluted areas (see e.g.
6 Eisinger and Burrows, 1998; Krotkov et al., 2006; Lee et al., 2009; Nowlan et al., 2011;
7 Fioletov et al., 2013; Yang et al., 2013; Boynard et al., 2014). During the last decade, a new
8 remote sensing technique called MAX-DOAS (Multi-Axis Differential Optical Absorption
9 Spectroscopy) has been developed, providing information on both VCD and vertical
10 distribution of trace gases in the troposphere (Hönninger et al., 2004; Platt and Stutz, 2008). It
11 is based on the measurement of sunlight scattered at multiple elevation angles towards the
12 horizon, thus increasing the sensitivity to absorbers present close to the ground compared to
13 the zenith viewing geometry (Hönninger et al., 2004). MAX-DOAS studies published so far
14 have been mainly focused on the retrieval of NO_2 (e.g. Wittrock et al., 2004; Vlemmix et al.,
15 2010; Frins et al., 2012; Hendrick et al., 2014; Ma et al., 2013; Wang et al., 2014), halogen
16 oxides like BrO and IO (e.g. Frieß et al., 2011; Großmann et al., 2013), formaldehyde (e.g.
17 Heckel et al., 2005; Wagner et al., 2011), and aerosols (e.g. Wagner et al., 2004; Frieß et al.,
18 2006; Clémer et al., 2010). A lot of work has been done on MAX-DOAS measurements of
19 volcanic SO_2 (e.g. Bobrowski et al., 2007a; Galle et al., 2010), but so far, only a few studies
20 deal with MAX-DOAS observations of this species in polluted area (e.g. Irie et al., 2011; Lee
21 et al., 2008; Wu et al., 2013), despite the fact that as for other trace gases like NO_2 , HCHO,
22 and BrO, the combination of both surface concentration and VCD retrievals makes
23 MAX-DOAS a useful technique for validating SO_2 satellite data.

24 Here we present three years (March 2010-February 2013) of continuous MAX-DOAS SO_2
25 observations at the Xianghe Observatory, China (39.75°N , 116.96°E), located at about 50 km
26 southeast of Beijing, at the borders among Beijing, Tangshan and Tianjin (see Fig. 1). The
27 station is operated by the Institute of Atmospheric Physics (IAP)/ Chinese Academy of
28 Sciences (CAS) while the MAX-DOAS instrument was developed by the Belgian Institute for

1 Space Aeronomy (BIRA-IASB) and validated in several intercomparison exercises, in
2 particular as part of the international Cabauw Intercomparison of Nitrogen Dioxide measuring
3 Instruments (CINDI, Roscoe et al., 2010) and more recently a national Chinese MAX-DOAS
4 instruments intercomparison campaign held in Xianghe (Wang et al., 2013). SO₂
5 MAX-DOAS observations are used here in combination with in-situ measurements as well as
6 conventional meteorological data (temperature, humidity, wind direction and speed) to
7 investigate the seasonal and diurnal cycles of SO₂ vertical profiles and VCDs. The paper is
8 divided into three main Sections. In Sect. 2, the SO₂ measurements are described, including
9 the DOAS analysis, vertical profile retrieval, and retrieval verification through comparison
10 with in situ data. The seasonal and diurnal cycles of SO₂, and the relationship between SO₂
11 and aerosols are investigated in Sect. 3. Finally, conclusions are given Sect. 4.

12 **2 Data**

13 **2.1 Instrument**

14 The MAX-DOAS instrument operated at the Xianghe Observatory consists of three
15 components: a thermo-regulated box containing two spectrometers, an optical head mounted
16 on a sun tracker, and two computers for instrument control and data storage (Clémer et al.,
17 2010). The optical head and the two spectrometers are linked by two-way splitter optical
18 fibers (Clémer et al., 2010; Wang et al., 2013). This setup is capable of measuring scattered as
19 well as direct sunlight. One spectrometer works in the UV region (300 to 390 nm) and its
20 instrumental function is close to a Gaussian with a full width at half maximum (FWHM) of
21 0.4 nm. The other spectrometer covers the visible wavelength range from 400 to 720 nm with
22 a FWHM equal to 0.9 nm. During the observation, the azimuth direction of the telescope is
23 fixed to the North. A full MAX-DOAS scan consists of 9 elevation viewing angles (2°, 4°, 6°,
24 8°, 10°, 12°, 15°, 30°, and 90°) and lasts about 15 minutes (Clémer et al., 2010). The 3-year
25 data set investigated in this study covers the March 2010 to February 2013 period.

1 2.2 DOAS analysis

2 Scattered-sunlight spectra measured at different elevation angles (EVAs) are analyzed using
3 the DOAS technique (Platt and Stutz, 2008) where high-frequency molecular absorption
4 structures in the UV and visible regions of the spectrum are exploited to detect and quantify a
5 number of key atmospheric gases such as SO₂.

6 In this work, the spectra obtained from MAX-DOAS observations are analyzed using the
7 QDOAS spectral-fitting software suite developed at BIRA-IASB
8 (<http://uv-vis.aeronomie.be/software/QDOAS/>). QDOAS calculates the SO₂ differential slant
9 column densities (DSCDs), which are defined as the difference between the trace-gas
10 concentration integrated along the effective light path and the amount of the absorber in a
11 measured reference spectrum. (MAX-)DOAS is recognized as a “self-calibrating” technique
12 because differential absorptions are measured and therefore the impact of possible
13 instrumental degradations can be largely removed by using appropriate reference spectra. In
14 contrast, in-situ instruments need to be optically and/or chemically calibrated on a regular
15 basis, especially when performing long-term measurements. For tropospheric studies, a zenith
16 spectrum is frequently chosen as reference, in this way also removing the contribution of the
17 stratosphere in off-axis DSCDs.

18 The SO₂ DOAS settings have been investigated through sensitivity tests on several key
19 parameters, such as wavelength interval, choice of absorption cross sections, polynomial
20 order, and intensity off-set terms. The selected settings are summarized in Table 1 and
21 described below.

22 SO₂ fitting windows ranging between 303 and 325 nm have generally been used in previous
23 studies (Bobrowski and Platt, 2007b; Lee et al., 2008; Galle et al., 2010; Irie et al., 2011). At
24 wavelengths shorter than 303 nm, the limiting factor is the strong ozone absorption which
25 interferes with SO₂, leading to lower signal to noise ratio. At wavelengths longer than 325 nm,
26 the SO₂ differential absorption signal becomes too weak. In order to identify the wavelength
27 interval which minimizes both random and systematic uncertainties on SO₂ retrieval, 6

1 wavelength intervals have been investigated. The results of these sensitivity tests for two
2 example days are presented in Figs. 2 and 3. On the first day (1st October 2011), the SO₂
3 content is minimum and stable in time. On the second day (4th October 2011), large variations
4 of the SO₂ content occur, so the ability of the different intervals to give consistent and stable
5 values can be verified. As can be seen, the 305-317.5 nm interval provides the lowest fitting
6 errors throughout the day and the smallest dependence on the solar zenith angle (SZA) for
7 both days. Due to the larger absorption and therefore interference by O₃ at large SZAs, it has
8 been decided to exclude measurements taken at SZAs larger than 75°. For these tests, the
9 following spectral signatures have been included: SO₂, O₃, NO₂, and the Ring effect (Grainger
10 and Ring, 1962; Chance and Spurr, 1997). Daily zenith-sky radiance spectra recorded around
11 local noon have been selected as reference. To account for the temperature dependence of the
12 ozone absorption, cross sections at 2 different temperatures (223°K and 243°K) were used
13 according to Van Roozendaal et al. (2006). A fifth-order polynomial is applied to fit the
14 low-frequency spectral structure due to Rayleigh and Mie scattering and instrumental effects.
15 Attempts to further adjust these settings, e.g. by adding BrO cross-section or by including
16 additional ozone correction terms according to Puķīte et al. (2010) were not successful (less
17 stable retrievals with larger noise on the SO₂ DSCDs).

18 Fig. 4 shows a typical example of a DOAS fit for SO₂ at 43° SZA. We see that fitting
19 residuals range in between -2×10^{-3} and 2×10^{-3} , corresponding to a root-mean-squares (RMS)
20 of 9×10^{-4} , which appears to be small in comparison to the SO₂ differential structures presented
21 in the lowest panel of the figure. The typical fitting uncertainty on SO₂ DSCDs is of about
22 $1-6 \times 10^{15}$ molec·cm⁻² (less than 10%), and for the case illustrated here, corresponds to 2%. For
23 near-noon conditions, the detection limit on the SO₂ DSCD can be conservatively estimated
24 as 3 times the one-sigma uncertainty on the slant column, which means approximately 3×10^{15}
25 molec·cm⁻². This detection limit is similar for the vertical columns estimated using the
26 geometrical approximation at 30° elevation (see Sect. 2.3). Vertical columns derived from the
27 full inversion generally have a smaller detection limit, owing to the gain in sensitivity
28 obtained when including near horizontal viewing measurements.

1 2.3 Profile retrieval

2 SO₂ vertical profiles are retrieved for each MAX-DOAS scan by applying the bePRO
3 profiling tool developed at BIRA-IASB (Cl mer et al., 2010; see also Hendrick et al., 2014) to
4 the corresponding off-axis minus zenith DSCDs measured at the different EVAs. bePRO is
5 based on the Optimal Estimation Method (Rodgers, 2000) and includes the LIDORT radiative
6 transfer model (RTM) as a forward model. A two-step approach is implemented in bePRO:
7 First, aerosol extinction profiles are retrieved from measured O₄ DSCDs. This step is needed
8 because the aerosols strongly influence the effective light path in the atmosphere and
9 therefore the optical density of trace gases like SO₂. Secondly, bePRO is applied to measured
10 trace-gas DSCDs using the retrieved aerosol extinction profiles for the radiative transfer
11 calculations (see below).

12 Both linear and non-linear iterative approaches have been implemented in our profiling
13 algorithm. For weak absorbers like NO₂, HCHO and SO₂, the linear method is selected (see
14 e.g. Hendrick et al., 2004). In case of strong absorbers like O₄, the non-linear iterative
15 approach is used:

$$16 \quad \mathbf{x}_{i+1} = \mathbf{x}_i + (\mathbf{S}_a^{-1} + \mathbf{K}_i^T \mathbf{S}_\epsilon^{-1} \mathbf{K}_i)^{-1} \cdot [\mathbf{K}_i^T \mathbf{S}_\epsilon^{-1} (\mathbf{y} - \mathbf{F}(x_i)) - \mathbf{S}_a^{-1} (\mathbf{x}_i - \mathbf{x}_a)] \quad (1)$$

17 where \mathbf{y} is the observation vector with the DSCDs at the different EVAs, \mathbf{F} is the forward
18 model describing the physics of the measurements, \mathbf{K} is the weighting function, expressing
19 the sensitivity of the measurements to changes in the aerosol extinction or SO₂ vertical profile
20 and calculated on-line by the LIDORT RTM, \mathbf{S}_ϵ is the measurement uncertainty covariance
21 matrix, \mathbf{x}_a and \mathbf{S}_a are the a priori vertical profile and its corresponding error covariance matrix.
22 A priori information is needed in the OEM method in order to indirectly reject unrealistic
23 solutions compatible with the measurements. Another important quantity in the OEM is the
24 averaging kernel matrix \mathbf{A} , which represents the sensitivity of the retrieval to the true state.
25 More specifically, each element \mathbf{A}_{ij} in the matrix \mathbf{A} describes the sensitivity of the retrieval at
26 i^{th} level to the true states at the different altitude levels j . Furthermore, the trace of the matrix

1 **A** gives the degrees of freedom of signal (DFS), which corresponds to the number of
2 independent pieces of information contained in the measurements. Due to the nonlinearity of
3 the inverse problem in case of aerosols, the solution to equation (1) must be iterated until
4 satisfactory convergence is achieved between measured DSCDs and those calculated using
5 the retrieved aerosol extinction vertical profile.

6 Regarding the choice of the a priori profile x_a , exponentially decreasing a priori SO₂ and
7 aerosol extinction profiles with a fixed scaling height of 0.5km have been constructed
8 according to the following expression:

$$9 \quad X_a(z) = \frac{VCD_a}{SH} e^{-\frac{z}{SH}} \quad (2)$$

10 where $x_a(z)$ is the a priori profile, SH the scaling height (0.5 km), and VCD_a (AOD_a) is the a
11 priori vertical column density (aerosol optical depth). For each scan, VCD_a is derived using
12 the geometrical approximation method, i.e. the SO₂ layer is assumed to be located below the
13 scattering altitude at 30° EVA, so that tropospheric SO₂ VCDs can be derived by applying a
14 geometrical air mass factor (AMF) to measured 30° EVA DSCDs (Hönninger et al., 2004;
15 Brinkma et al., 2008; see also Hendrick et al., 2014). In case of aerosols, a fixed AOD of 0.2
16 is used. Since the DOAS fitting intervals are different for SO₂ and aerosols, the aerosol
17 extinction profiles utilized as input for the calculation of SO₂ weighting functions have been
18 derived by directly converting the aerosol profiles retrieved in the 338-370 nm wavelength
19 range to the 305-317.5 nm interval using the Ångström exponents (Cachorro et al., 2000)
20 retrieved from collocated CIMEL/AERONET sunphotometer measurements (Holben et al.,
21 1998; see <http://aeronet.gsfc.nasa.gov>):

$$22 \quad \text{Extinction}(z, 313 \text{ nm}) = \text{Extinction}(z, 360 \text{ nm}) \times (313/360)^{-\alpha} \quad (3)$$

23 where z is the altitude and α is the Ångström exponent.

24 The 340-440 nm exponents are used in a first approximation since values for a wavelength
25 range closer to the SO₂ fitting interval (305-317.5 nm) are not available so far. The

1 corresponding mean scaling factor for the March 2010 – February 2013 period is of 1.16 ± 0.06 .

2 The single scattering albedo and phase function of aerosols at 360 nm required by bePRO for
3 retrieving aerosol extinction profiles are calculated off-line based on the aerosol size
4 distribution and refractive index retrieved from the same CIMEL/AERONET sunphotometer
5 measurements as above. The temperature-pressure profiles are obtained from the US standard
6 atmosphere. S_e and S_a matrices are similar as in Cl mer et al. (2010) and Hendrick et al.
7 (2014). S_e is a diagonal matrix, with variances equal to the square of the DOAS fitting error.
8 For S_a , the diagonal element corresponding to the lowest layer, $S_a(1,1)$, is set equal to the
9 square of a scaling factor β times the maximum partial VCD (AOD) of the profiles. Here
10 $\beta=0.4$ for SO_2 and 0.2 for aerosol. The other diagonal elements decrease linearly with altitude
11 down to $0.2 \times S_a(1,1)$. The off-diagonal terms in S_a , were set using Gaussian functions as
12 follows:

$$S_a(i, j) = \sqrt{S_a(i, i)S_a(j, j) \exp(-\ln(2)\left(\frac{z_i - z_j}{\gamma}\right)^2)}$$

(4)

14 where z_i and z_j are the altitudes of i^{th} and j^{th} levels, respectively. The correlation length is set to
15 0.1 km for SO_2 and 0.05km for aerosol in order to optimize the DFS.

16 The retrieval altitude grid is also the same as in Cl mer et al. (2010) and Hendrick et al.
17 (2014), i.e. ten layers of 200 m thickness between 0 and 2 km, two layers of 500 m between 2
18 and 3 km and 1 layer between 3 and 4 km.

19 Fig. 5 shows an example of a SO_2 profile retrieval (Xianghe, 29 September 2010, 10:15 LT).
20 Fig. 5(a) compares the a priori and retrieved profiles; Fig. 5(b) shows an example of fit results,
21 i.e. the comparison between measured DSCDs and those calculated from the retrieved profile.
22 The quality of the profile retrieval is checked for each scan by calculating the relative Root
23 Mean Square Error (RMS) between observed and calculated DSCDs. This RMS corresponds
24 to the standard RMS expressed in molec/cm^2 divided by the mean DSCD of the scan. All
25 retrievals based on the following selection criteria have been selected: $\text{RMS} < 15\%$, $\text{DFS} > 0.7$,
26 and negative values not allowed. For each year, the number of selected retrievals using these

1 criteria reaches ~70% of the total number of scans.

2 Also shown in Fig. 5 are the smoothing and noise errors (c) and the averaging kernels (d).

3 Regarding the errors, the smoothing error limits the ability of the retrieval to obtain solutions

4 far from the a priori, while the noise error is related to the propagation of the noise in the

5 measurements into the retrieval (Rodgers, 2000). From Fig. 5(c), we see that the smoothing

6 error is significantly larger than the noise error, except in the 0-200m layer. The averaging

7 kernels show that the retrieval is mainly sensitive to the layer close to the surface in addition

8 to the total vertical column. In this example, the DFS is about 2.4, suggesting that two

9 independent pieces of information can be determined from the measurements.

10 The error budget is presented in Table 2. Uncertainty related to aerosols is estimated by

11 retrieving SO₂ profiles using wavelength-converted retrieved aerosol profiles plus their

12 corresponding error (i.e. the sum of smoothing and noise errors plus a 20% error due to the

13 uncertainty on the O₄ cross sections (Cl mer et al., 2010)) as input and comparing the results

14 to the standard retrievals. The uncertainty on the SO₂ cross sections is set to 5%, as suggested

15 by Vandaele et al. (1994). The uncertainty on the a priori profiles is estimated by taking SH =

16 1 km in Eq. (2) instead of 0.5 km in the standard retrieval. The total uncertainty is calculated

17 by adding the different terms in Gaussian quadrature.

18 Monthly-mean SO₂ profiles are shown in Fig. 6. There is a maximum SO₂ concentration in

19 the 200-400m layer for each profile, except in summer where the maximum is located near

20 the surface. The largest vertical gradient is observed in February and November, the minimum

21 in July and August. This is mainly due to the fact that the SO₂ emissions are the highest in

22 February and November. This will be discussed in detail below.

23 Fig. 7 shows the seasonal mean of diurnal cycle of DFS. The diurnal distribution in any

24 season shows a single peak at mid-day due to the fact that the retrieval error at late evening or

25 early morning overweights that at noon. If we compare the DFS around noon among the

26 different seasons, values in summer are lower compared to the other seasons due to the lower

27 SO₂ amounts associated with larger uncertainties observed during this period.

1

2 **2.4 SO₂ surface concentration retrieval verification**

3 For verification purpose, our retrieved SO₂ surface concentrations have been compared to
4 measurements from a modified commercial in-situ instrument, based on pulsed UV
5 fluorescence technology (Thermo Environmental Instruments Model 43C) (Li et al., 2007).
6 Comparison results for December 2011 when the in-situ instrument was freshly calibrated are
7 shown in Fig. 8. Hourly and daily averages of SO₂ concentration are plotted in Fig. 8(a) and
8 (b), respectively. A good agreement is obtained with a correlation coefficient of 0.86 and a
9 slope of 0.95.

10 In Fig. 9, the daytime variations of the MAX-DOAS and in-situ SO₂ surface concentration are
11 compared for 9 continuous days. A very good agreement is found between both data sets,
12 indicating the good overall reliability and the robustness of our MAX-DOAS retrievals.

13 **3 Results and discussion**

14 Based on the SO₂ profiles retrieved for the period from March 2010 to February 2013, we
15 have investigated the daily and seasonal variations of the SO₂ VCD and surface concentration
16 and the possible influence of meteorological conditions, including atmospheric stability, wind
17 direction and speed. We have adopted the following convention for the seasons: MAM, JJA,
18 SON, and NJF for spring, summer, autumn, and winter, respectively.

19 **3.1 Seasonal variation of SO₂**

20 Fig. 10(a) shows that the SO₂ VCD is highly correlated with concentration close to the ground
21 (correlation coefficient of 0.85). From Fig. 10(b), we see that the temporal evolutions of SO₂
22 VCD and concentration are very similar, consistent with the fact that the SO₂ emission
23 sources are located near the ground.

24 The monthly averaged SO₂ VCD and surface concentrations are shown in Fig. 11. Both show

1 a marked seasonal signature with a maximum in winter and a minimum in summer, implying
2 that SO₂ originates mainly from human sources rather than natural ones (Lin et al., 2011).
3 Generally, the fluctuations of any atmospheric pollutant in a region of interest can be mainly
4 attributed to three factors: emission level, residence time, and atmospheric transport (Wang et
5 al., 2010; Lin et al., 2011). From the perspective of emission level, firstly, owing to enhanced
6 domestic heating and associated coal and oil consumption in winter, the heating-related
7 emissions of SO₂ are much larger during this period than in summer. Secondly, the residence
8 time, defined as the rate of removal mechanisms, also plays an important role in determining
9 the seasonal variation of SO₂ concentrations (Lee et al., 2011). Processes responsible for the
10 removal of SO₂ involve dry and wet deposition and homogeneous or inhomogeneous
11 gas-phase reactions leading to the production of H₂SO₄ or sulfate (Tu et al., 2004). As shown
12 in Fig. 12, the relative humidity is lower in winter, so that the removal of SO₂ through wet
13 deposition is not as substantial as in summer. Thirdly, the transport can also influence the
14 evolution of SO₂ at a given location. Although in winter the wind is stronger at Xianghe, the
15 emissions also increase during the same period. **In addition, the reduced atmospheric
16 boundary layer height and frequent temperature inversion events result in larger surface
17 concentrations due to an accumulation of SO₂ in the lower troposphere (Meng et al., 2009).** In
18 summary, the aforementioned three factors jointly lead to the observed seasonal pattern of
19 SO₂ concentration in Xianghe.

20 From Fig. 11, we see that the amount of SO₂ strongly increases in November with respect to
21 October, as a consequence of increasing domestic heating (November is the beginning of the
22 domestic heating season). Moreover, the higher wind speed observed in December (see Fig.
23 12) leads to a decrease of SO₂ during this month due to more efficient diffusion and dilution
24 effects. Finally, it is also noticeable that SO₂ in January 2011 is remarkably lower than that in
25 other years. This will be further discussed below.

26 **3.2 Impact of meteorological conditions**

27 Because of the high correlation coefficient and similar seasonal variations of the SO₂ VCD

1 and concentration, we decided to investigate the impact of meteorological conditions on
2 VCDs only. The variation of the SO₂ VCD is closely linked not only to the spatial distribution
3 of emission sources but also to meteorological conditions including wind (speed and direction)
4 and precipitation. As shown in Fig. 12, in general, the variations of temperature and humidity
5 appear to exhibit similar behavior from year to year. This suggests that the contribution of the
6 wind speed and direction as driver for the SO₂ VCD variation is probably different over the
7 different years investigated here. We further explore the relationship between SO₂ and wind
8 (speed and direction), as displayed in Fig. 13. It can be seen that the amount of SO₂ is strongly
9 dependent on the wind direction (Fig. 13a): high VCDs are prominent when the winds blow
10 from the east, because Tangshan, a heavy industrial city releasing large amounts of SO₂, is
11 situated to the east of Xianghe (see Fig. 1); in contrast, the northwest direction corresponds to
12 a minimum in SO₂ VCD, since it is a mountain area, characterized by much less emissions
13 than in Xianghe. The wind therefore contributes significantly to the dispersion of the
14 pollutants, as expected. Regarding the dependence of the SO₂ VCD on wind speed, Fig. 13(b)
15 shows that the VCD is almost constant with wind speed for the E and SW, which means that
16 no good dispersion happens with the wind from these directions, since high-emission
17 industrial areas and Tangshan are located to the southwest and east of Xianghe, respectively.
18 In contrast, an anti-correlation is observed for NE/NNE, NW, and SE, which means that the
19 wind from these directions corresponding to less polluted areas can efficiently disperse
20 pollutants. In addition, the SO₂ content at Xianghe is more sensitive to the emission sources in
21 Tangshan (E) than in Beijing (WNW), which is consistent with the fact that Beijing has taken
22 regulatory actions to reduce air pollution through traffic-control measures and the closure of
23 heavy polluting industries initiated before the 2008 Olympic Games (Yu et al., 2010).

24 The annual cycles of SO₂ are generally in good agreement among the different years.
25 However, the SO₂ VCD in January 2011 drastically deviates by up to 30% from the values
26 during the same month in 2012 and 2013, which is also the case in May 2012. Wind roses in
27 Fig. 14 reveal that the inter-annual variability of wind speed and direction is responsible for
28 the significantly different SO₂ VCD in January 2011. During that month, the frequency of

1 north-west winds reaches 70% and wind speed predominantly exceed 5 m.s^{-1} . As mentioned
2 above, the strong northwesterly wind favors the atmospheric dispersion of pollutants.
3 Consequently, the SO_2 VCDs are generally lower than 4×10^{16} molec. cm^{-2} . For January 2012
4 and 2013, uniformly distributed wind on each side and low velocity ($<5\text{ m.s}^{-1}$,
5 frequency $>50\%$) jointly result in relatively high SO_2 VCDs compared to January 2011.
6 Similar features can explain the May 2012 case.

7 **3.3 Diurnal Cycle**

8 In Fig. 15, we further compare the diurnal cycles of SO_2 VCDs for the different seasons.
9 Since the sunshine duration is different in the four seasons, the available time period for
10 MAX-DOAS observations also differs: 7:30—17:30 in spring and autumn, 6:30—18:30 in
11 summer, and 8:30—16:30 in winter. As can be seen, the diurnal cycles for all years are very
12 consistent, especially in summer. The retrieved SO_2 VCDs in autumn 2011 and spring 2012
13 are significantly higher than those during the same period of the other years due to the
14 anomalous VCD values in November 2011 and May 2012. Furthermore, the amplitude of the
15 SO_2 VCD diurnal cycle, which shows a minimum at noon and a maximum in the morning and
16 late afternoon, is larger in winter. **This can be explained a strengthened diurnal variation of
17 emission sources during this period (Meng et al., 2009).**

18 It should be noted that similar investigations have been done for NO_2 (Wang et al., 2014). One
19 can conclude that both NO_2 and SO_2 display a similar seasonal variation and are impacted in
20 the same way by meteorological conditions. However, SO_2 abundances are always higher than
21 NO_2 ones and their diurnal cycles are different, especially in winter and summer: SO_2 has a
22 more pronounced diurnal cycle than NO_2 in winter which is in line with the known diurnal
23 cycle of burning of fossil fuels for heating and atmospheric stability, and the photochemical
24 reaction activity leads to an obvious decrease of NO_2 during daytime in summer (Wang et al.,
25 2008; Meng et al., 2009; Lin et al., 2011).

3.4 Relationship between SO₂ and aerosols

SO₂ is known as a major aerosol precursor through its conversion into sulfates and sulfuric acid by reaction with OH (see e.g. Ma et al., 2012). Since aerosol extinction profiles are retrieved in the first step of the SO₂ retrieval (see Sect. 2.3), our data set offers a unique opportunity to investigate the relationship between SO₂ emission and aerosol production in the Beijing suburban area.

Fig. 16 shows monthly scatter plots of the SO₂ concentration versus aerosol extinction coefficient retrieved in the 0-200m layer for the March 2010 – February 2013 period. A strong correlation (correlation coefficients in the 0.6-0.9 range) is obtained in JFM and OND while a significantly lower correlation is observed in late spring/summer with correlation coefficients around 0.3 in JJA. Similar features are found from the scatter plots of SO₂ VCD versus AOD (not shown here). The marked seasonality of the correlation between SO₂ and aerosols is further illustrated in Fig. 17 where monthly correlation coefficients for both surface concentration and integrated column are reported. The positive correlation (>0.2) observed throughout the year indicates that in most cases, high pollution events in Xianghe are associated with enhanced SO₂ and aerosol levels (Chan and Yao, 2008; Li et al., 2007). The higher correlation coefficients obtained in winter (>0.6) suggest that anthropogenic SO₂ plays a more significant role in the aerosols formation during this period of the year due to its larger concentration and lower temperatures favoring the formation of sulfates (Lin et al., 2012). In late spring/summer, the Beijing area is also strongly influenced by other sources of aerosols, especially particles emitted from massive agricultural fires in the surrounding region (Xia et al., 2013) as well as dust particles transported from the Kumutage and Taklimakan deserts in western China and from the Mongolian deserts (Yu et al., 2009). In combination to the lower SO₂ concentration, this could explain the significantly weaker correlation between anthropogenic SO₂ and aerosols obtained in JJA. However, measurements of the chemical composition of aerosols in Xianghe would be needed to further support our findings.

1 **4 Summary and conclusions**

2 Tropospheric SO₂ vertical profiles and corresponding column densities at the Xianghe station
3 have been retrieved by applying an OEM-based profiling tool to continuous ground-based
4 MAX-DOAS observations from March 2010 to February 2013. The 305-317.5 nm
5 wavelength range was found to be the most suitable fitting window for near-noon DOAS
6 analysis of SO₂. For verification purpose, retrieved SO₂ surface concentrations have been
7 compared to collocated in-situ data. An excellent agreement was found, with correlation
8 coefficient and slope close to 0.9, **indicating the good** reliability and robustness of our
9 retrievals.

10 These MAX-DOAS measurements have been used to investigate the seasonal and diurnal
11 cycles of SO₂ vertical columns and surface concentrations, in combination with conventional
12 meteorological data (temperature, humidity, and wind speed and direction). Regarding the
13 seasonal variation, both VCD and surface concentrations exhibit the same patterns, with a
14 maximum in winter (February) and a minimum in summer (July), in accordance with the large
15 emissions due to domestic heating in winter. The high levels of SO₂ during the cold season are
16 further enhanced by the weakness of the wet deposition mechanism and, **in case of surface**
17 **concentration**, by the frequent temperature-inversion events occurring during this period,
18 favoring the accumulation of SO₂ in the atmospheric layers close to the ground. The variation
19 of the SO₂ amount in Xianghe is also found to be largely driven by wind speed and direction.
20 In the case of east or southwest wind, the VCD at the station **remains almost constant** with the
21 increase of wind speed, since the city of Tangshan and heavy polluting industries are located
22 to the east and southwest **of Xianghe, respectively. In contrast, an anti-correlation between**
23 **SO₂ VCD and wind speed is observed for NE/NNE, NW, and SE directions, which means the**
24 **wind from these directions can efficiently disperse the pollution in Xianghe.** With respect to
25 the diurnal cycle, larger SO₂ amounts are obtained in the early morning and late evening with
26 a minimum around noon, in line with the diurnal variation of pollutant emission and
27 atmospheric state. Moreover, the diurnal cycle is more pronounced during wintertime, mainly

1 due to the more marked diurnal variation of emission sources during this season. The
2 relationship between SO₂ and aerosols has been also investigated. A strong correlation
3 between both is found in winter but not in summer. This seasonality could be related to the
4 fact that anthropogenic SO₂ plays a more dominant role in the aerosol formation in winter
5 while in summer dust and biomass burning particles contribute more significantly to the
6 aerosol content in Xianghe, the latter being therefore less SO₂-dependent.

7 These three-year MAX-DOAS SO₂ measurements in Xianghe constitute a unique data set for
8 validating and improving space-borne observations over China, which is the region in the
9 world where anthropogenic SO₂ emissions are the largest (Yang et al., 2013; Boynard et al.,
10 2014). In particular, retrieved SO₂ vertical profiles can be used as a priori information for the
11 AMF calculation in satellite retrievals. Moreover, the combination of both integrated columns
12 and surface concentrations could provide useful information to make explicitly the link
13 between measured satellite columns and surface concentrations.

15 Acknowledgements

16 This work was supported by China Scholarship Council, the Special Scientific Research Fund
17 of Meteorological Public Welfare Profession of China (Grant No. GYHY201106045-52), and
18 the National Natural Science Foundation of China (Grant No. 41175030). We acknowledge
19 the Belgian Federal Science Policy Office, Brussels (AGACC-II project), and the funding
20 obtained from the EU 7th Framework Programme project NORS (contract 284421) and the
21 ESA CEOS Intercalibration project (ESA/ESRIN Contract 22202/09/I-EC). We would like
22 also to thank J.-F. Müller (Belgian Institute for Space Aeronomy) for helpful discussions.

1 **References**

- 2 **Bobrowski, N., von Glasow, R., Aiuppa, A., Inguaggiato, S., Louban, I., Ibrahim, O. W., and**
3 **Platt, U.: Reactive halogen chemistry in volcanic plumes, *J. Geophys. Res.*, 112, D06311,**
4 **doi:10.1029/2006JD007206, 2007a.**
- 5 **Bobrowski, N., and Platt, U.: SO₂/BrO ratios studied in five volcanic plumes, *J. Volcanol.***
6 ***Geotherm. Res.*, 166, 147-160, 2007b.**
- 7 Bogumil, K., Orphal, J., Homann, T., Voigt, S., Spietz, P., Fleischmann, O. C., Vogel, A.,
8 Hartmann, M., Bovensmann, H., Frerik, J., and Burrows, J. P.: Measurements of molecular
9 absorption spectra with the SCIAMACHY Pre- Flight Model: Instrument characterization
10 and reference spectra for atmospheric remote sensing in the 230–2380nm region, *J.*
11 *Photoch. Photobio. A*, 157, 167–184, 2003.
- 12 Boynard, A., Clerbaux, C., Clarisse, L., Safieddine, S., Pommier, M., Van Damme, M.,
13 Bauduin, S., Oudot, C., Hadji-Lazaro, J., Hurtmans, D., and Coheur, P.-F.: First
14 simultaneous space measurements of atmospheric pollutants in the boundary layer from
15 IASI: a case study in the North China Plain, *Geophys. Res. Lett.*, 41, 645-651, doi:
16 10.1002/2013GL058333, 2014.
- 17 Brinkma, E. J., Pinardi, G., Volten, H., Braak, R., Richter, A., Schonhardt, A., van
18 Roozendael, M., Fayt, C., Hermans, C., Dirksen, R. J., Vlemmix, T., Berkhout, A. J. C.,
19 Swart, D. P. J., Oetjen, H., Wittrock, F., Wagner, T., Ibrahim, O. W., de Leeuw, G.,
20 Moerman, M., Curier, R. L., Celarier, E. A., Cede, A., Knap, W. H., Veeffkind, J. P., Eskes,
21 H. J., Allaart, M., Rothe, R., Piters, A. J. M., and Levelt, P. F.: The 2005 and 2006
22 DANDELIONS NO₂ and aerosol intercomparison campaigns, *J. Geophys. Res.*, 113,
23 D16S46, doi: 10.1029/2007jd008808, 2008.
- 24 Cachorro, V. E., Durán, P., Vergaz, R., and de Frutos, A. M.: Measurements of the
25 atmospheric turbidity of the north-centre continental area in Spain: Spectral aerosol optical
26 depth and Ångström turbidity parameters, *J. Aerosol Sci.*, 31, 687-702, 2000.

- 1 Chan, C. K., and Yao, X.: Air pollution in mega cities in China, *Atmos. Environ.*, 42, 1-42,
2 2008.
- 3 Chance, K. V., and Spurr, R. J.: Ring effect studies: Rayleigh scattering, including molecular
4 parameters for rotational Raman scattering, and the Fraunhofer spectrum, *Applied Optics*,
5 36, 5224-5230, 1997.
- 6 Clémer, K., Van Roozendael, M., Fayt, C., Hendrick, F., Hermans, C., Pinardi, G., Spurr, R.,
7 Wang, P., and De Maziere, M.: Multiple wavelength retrieval of tropospheric aerosol
8 optical properties from MAXDOAS measurements in Beijing, *Atmos. Meas. Tech.*, 3,
9 863-878, 10.5194/amt-3-863-2010, 2010.
- 10 Eisinger, M., and Burrows, J. P.: Tropospheric sulfur dioxide observed by the ERS-2/GOME
11 instrument, *Geophys. Res. Lett.*, 25(22), 4177–4180, doi:10.1029/1998GL900128, 1998.
- 12 Fioletov, V. E., McLinden, C. A., Krotkov, N., Yang, K., Loyola, D. G., Valks, P., Theys, N.,
13 Van Roozendael, M., Nowlan, C. R., Chance, K., Liu, X., Lee, C., and Martin, R. V.:
14 Application of OMI, SCIAMACHY, and GOME-2 satellite SO₂ retrievals for detection of
15 large emission sources, *J. Geophys. Res.: Atmospheres*, 118(19), 11,399–11,418,
16 doi:10.1002/jgrd.50826, 2013.
- 17 Fleischmann, O. C., Hartmann, M., Burrows, J. P., and Orphal, J.: New ultraviolet absorption
18 cross-sections of BrO at atmospheric temperatures measured by time-windowing Fourier
19 transform spectroscopy, *J. Photoch. Photobio. A: Chemistry*, 168, 117-132, 2004.
- 20 Frieß, U., Monks, P. S., Remedios, J. J., Rozanov, A., Sinreich, R., Wagner, T., and Platt, U.:
21 MAX-DOAS O₄ measurements: A new technique to derive information on atmospheric
22 aerosols: 2. Modeling studies, *J. Geophys. Res.*, 111, D14203, doi: 10.1029/2005jd006618,
23 2006.
- 24 Frieß, U., Sihler, H., Sander, R., Pöhler, D., Yilmaz, S., and Platt, U.: The vertical distribution
25 of BrO and aerosols in the Arctic: Measurements by active and passive differential optical
26 absorption spectroscopy, *J. Geophys. Res.*, 116, D00R04, doi: 10.1029/2011JD015938,

1 2011.

2 Frins, E., Osorio, M., Casaballe, N., Belsterli, G., Wagner, T., and Platt, U.:
3 DOAS-measurement of the NO₂ formation rate from NO_x emissions into the atmosphere,
4 Atmos. Meas. Tech., 5, 1165-1172, doi: 10.5194/amt-5-1165-2012, 2012.

5 Galle, B., Johansson, M., Rivera, C., Zhang, Y., Kihlman, M., Kern, C., Lehmann, T., Platt, U.,
6 Arellano, S., and Hidalgo, S.: Network for Observation of Volcanic and Atmospheric
7 Change (NOVAC)-A global network for volcanic gas monitoring: Network layout and
8 instrument description, *J. Geophys. Res.*, 115, D05304, doi:10.1029/2009JD011823, 2010.

9 Gauderman, W. J., McConnell, R., Gilliland, F., London, S., Thomas, D., Avol, E., Vora, H.,
10 Berhane, K., Rappaport, E. B., and Lurmann, F.: Association between air pollution and
11 lung function growth in southern California children, *Am. J. Resp. Crit. Care.*, 162,
12 1383-1390, 2000.

13 Grainger, J., and Ring, J.: Anomalous Fraunhofer line profiles, *Nature*, 193, p. 762, 1962.

14 Großmann, K., Frieß, U., Peters, E., Wittrock, F., Lampel, J., Yilmaz, S., Tschritter, J.,
15 Sommariva, R., von Glasow, R., Quack, B., Krüger, K., Pfeilsticker, K., and Platt, U.:
16 Iodine monoxide in the Western Pacific marine boundary layer, *Atmos. Chem. Phys.*, 13,
17 3363-3378, doi: 10.5194/acp-13-3363-2013, 2013.

18 Hönninger, G., Friedeburg, C. v., and Platt, U.: Multi axis differential optical absorption
19 spectroscopy (MAX-DOAS), *Atmos. Chem. Phys.*, 4, 231-254, 2004.

20 Heckel, A., Richter, A., Tarsu, T., Wittrock, F., Hak, C., Pundt, I., Junkermann, W., and
21 Burrows, J. P.: MAX-DOAS measurements of formaldehyde in the Po-Valley, *Atmos.*
22 *Chem. Phys.*, 5, 909-918, 2005.

23 Hendrick, F., Barret, B., Van Roozendaal, M., Boesch, H., Butz, A., De Mazière, M., Goutail,
24 F., Hermans, C., Lambert, J.-C., Pfeilsticker, K., and Pommereau, J.-P.: Retrieval of
25 nitrogen dioxide stratospheric profiles from ground-based zenith-sky UV-visible
26 observations: Validation of the technique through correlative comparisons, *Atmos. Chem.*

- 1 Phys., 4, 2091-2106, 2004.
- 2 Hendrick, F., Müller, J.-F., Clémer, K., Wang, P., Mazière, M. D., Fayt, C., Gielen, C.,
3 Hermans, C., Ma, J., Pinardi, G., Stavrou, T., Vlemmix, T., and Van Roozendael, M.:
4 Four years of ground-based MAX-DOAS observations of HONO and NO₂ in the Beijing
5 area, *Atmos. Chem. Phys.*, 14, 765-781, 2014.
- 6 Hermans, C., Vandaele, A., Fally, S., Carleer, M., Colin, R., Coquart, B., Jenouvrier, A., and
7 Merienne, M.-F.: Absorption cross-section of the collision-induced bands of oxygen from
8 the UV to the NIR, in: *Weakly interacting molecular pairs: unconventional absorbers of*
9 *radiation in the atmosphere*, Springer, 193-202, 2003.
- 10 Holben, B., Eck, T., Slutsker, I., Tanre, D., Buis, J., Setzer, A., Vermote, E., Reagan, J.,
11 Kaufman, Y., and Nakajima, T.: AERONET—A federated instrument network and data
12 archive for aerosol characterization, *Remote Sens. Environ.*, 66, 1-16, 1998.
- 13 Irie, H., Takashima, H., Kanaya, Y., Boersma, K. F., Gast, L., Wittrock, F., Brunner, D., Zhou,
14 Y., and Van Roozendael, M.: Eight-component retrievals from ground-based MAX-DOAS
15 observations, *Atmos. Meas. Tech.*, 4, 1027-1044, doi:10.5194/amt-4-1027-2011, 2011.
- 16 Krotkov, N. A., Carn, S. A., Krueger, A. J., Bhartia, P. K., and Yang, K.: Band Residual
17 Difference Algorithm for Retrieval of SO₂ From the Aura Ozone Monitoring Instrument
18 (OMI), *IEEE Trans. Geosci. Remote Sens.*, 44(5), 1259–1266, 2006.
- 19 Lee, C., Richter, A., Lee, H., Kim, Y. J., Burrows, J. P., Lee, Y. G., and Choi, B. C.: Impact
20 of transport of sulfur dioxide from the Asian continent on the air quality over Korea during
21 May 2005, *Atmos. Environ.*, 42, 1461-1475, 2008.
- 22 Lee, C., Martin, R. V., van Donkelaar, A., O’Byrne, G., Krotkov, N., Richter, A., Huey, L.G.,
23 and Holloway, J. S.: Retrieval of vertical columns of sulfur dioxide from SCIAMACHY and
24 OMI: Air mass factor algorithm development, validation, and error analysis, *J. Geophys.*
25 *Res.*, 114(D22), D22303, doi:10.1029/2009JD012123, 2009.

- 1 Lee, C., Martin, R. V., van Donkelaar, A., Lee, H., Dickerson, R. R., Hains, J. C., Krotkov, N.,
2 Richter, A., Vinnikov, K. , and Schwab, J. J.: SO₂ emissions and lifetimes: Estimates from
3 inverse modeling using in situ and global, space - based(SCIAMACHY and OMI)
4 observations, *J. Geophys. Res.*, 116, D06304, doi:10.1029/2010JD014758, 2011.
- 5 Li, C., Marufu, L. T., Dickerson, R. R., Li, Z., Wen, T., Wang, Y., Wang, P., Chen, H., and
6 Stehr, J. W.: In situ measurements of trace gases and aerosol optical properties at a rural
7 site in northern China during East Asian Study of Tropospheric Aerosols: An International
8 Regional Experiment 2005, *J. Geophys. Res.*, 112, D22S04, doi: 10.1029/2006JD007592,
9 2007.
- 10 Lin, W., Xu, X., Ge, B., and Liu, X.: Gaseous pollutants in Beijing urban area during the
11 heating period 2007–2008: variability, sources, meteorological, and chemical impacts,
12 *Atmos. Chem. Phys.*, 11, 8157-8170, 2011.
- 13 Lin, M., Tao, J., Chan, C.-Y., Cao, J.-J., Zhang, Z.-S., Zhu, L.-H., and Zhang, R.-J.:
14 Characterization of regression relationship between recent air quality and visibility changes
15 in megacities at four haze regions of China, *Aerosol and Air Quality Research*, 12 (6),
16 1049-1061, doi: 10.4209/aaqr.2011.11.0220, 2012.
- 17 Ma, J. Z., Beirle, S., Jin, J. L., Shaiganfar, R., Yan, P., and Wagner, T.: Tropospheric NO₂
18 vertical column densities over Beijing: results of the first three years of ground-based
19 MAX-DOAS measurements (2008-2011) and satellite validation, *Atmos. Chem. Phys.*, 13,
20 1547-1567, doi: 10.5194/acp-13-1547-2013, 2013.
- 21 Ma, J. Z., Xu, X. B., Zhao, C. S., and Yan, P.: A review of atmospheric chemistry research in
22 China: Photochemical smog, haze pollution, and gas-aerosol interactions, *Adv. Atmos. Sci.*,
23 29, 1006-1026, 2012.
- 24 Meller, R., and Moortgat, G. K.: Temperature dependence of the absorption cross sections of
25 formaldehyde between 223 and 323 K in the wavelength range 225-375 nm, *J. Geophys.*
26 *Res.*, 105, 7089-7101, 2000.

- 1 Meng, X., Wang, P., Wang, G., Yu, H., and Zong, X.: Variation and transportation
2 characteristics of SO₂ in winter over Beijing and its surrounding areas, *Climatic and*
3 *Environmental Research (in Chinese)*, 14, 309-317, 2009.
- 4 Nowlan, C. R., Liu, X., Chance, K. V, Cai, Z., Kurosu, T. P., Lee, C., and Martin, R. V. :
5 Retrievals of sulfur dioxide from the Global Ozone Monitoring Experiment 2 (GOME-2)
6 using an optimal estimation approach: Algorithm and initial validation, *J. Geophys. Res.*,
7 116(D18), D18301, doi:10.1029/2011JD015808, 2011.
- 8 Platt, U., and Stutz, J.: *Differential Optical Absorption Spectroscopy (DOAS): Principles and*
9 *applications*, ISBN 978-3-540-21193-8, Springer, Berlin-Heidelberg, 2008.
- 10 Puķīte, J., Kühl, S., Deutschmann, T., Platt, U., and Wagner, T.: *Extending differential optical*
11 *absorption spectroscopy for limb measurements in the UV*, *Atmos. Meas. Tech.*, 3, 631-653,
12 2010.
- 13 Rodgers, C. D.: *Inverse methods for atmospheric sounding : theory and practice*, World
14 *Scientific Publishing*, Singapore-New Jersey-London-Hong Kong, 2000.
- 15 Roscoe, H. K., Van Roozendaal, M., Fayt, C., du Piesanie, A., Abuhassan, N., Adams, C.,
16 Akrami, M., Cede, A., Chong, J., Clemer, K., Friess, U., Ojeda, M. G., Goutail, F., Graves,
17 R., Griesfeller, A., Grossmann, K., Hemerijckx, G., Hendrick, F., Herman, J., Hermans, C.,
18 Irie, H., Johnston, P. V., Kanaya, Y., Kreher, K., Leigh, R., Merlaud, A., Mount, G. H.,
19 Navarro, M., Oetjen, H., Pazmino, A., Perez-Camacho, M., Peters, E., Pinardi, G.,
20 Puentedura, O., Richter, A., Schonhardt, A., Shaiganfar, R., Spinei, E., Strong, K.,
21 Takashima, H., Vlemmix, T., Vrekoussis, M., Wagner, T., Wittrock, F., Yela, M., Yilmaz, S.,
22 Boersma, F., Hains, J., Kroon, M., Piters, A., and Kim, Y. J.: Intercomparison of slant
23 column measurements of NO₂ and O₄ by MAX-DOAS and zenith-sky UV and visible
24 spectrometers, *Atmos. Meas. Tech.*, 3, 1629-1646, doi: 10.5194/amt-3-1629-2010, 2010.
- 25 Tu, F. H., Thornton, D. C., Bandy, A. R., Carmichael, G. R., Tang, Y., Thornhill, K. L., Sachse,
26 G. W., and Blake, D. R.: Long-range transport of sulfur dioxide in the central Pacific, *J.*

- 1 Geophys. Res., 109, D15S08, doi:10.1029/2003JD004309, 2004.
- 2 Vandaele, A., Simon, P. C., Guilmot, J. M., Carleer, M., and Colin, R.: SO₂ absorption cross
3 section measurement in the UV using a Fourier transform spectrometer, J. Geophys. Res.,
4 99, D12, 25599-25605, 1994.
- 5 Vandaele, A. C., Hermans, C., Simon, P. C., Carleer, M., Colin, R., Fally, S., Merienne, M.-F.,
6 Jenouvrier, A., and Coquart, B.: Measurements of the NO₂ absorption cross-section from
7 42 000 cm⁻¹ to 10 000 cm⁻¹(238–1000 nm) at 220 K and 294 K, Journal of Quantitative
8 Spectroscopy and Radiative Transfer, 59, 171-184, 1998.
- 9 Van Roozendael, M., Loyola, D., Spurr, R., Balis, D., Lambert, J.-C., Livschitz, Y., Valks, P.,
10 Ruppert, T., Kenter, P., Fayt, C., and Zehner, C.: Ten years of GOME/ERS-2 total ozone
11 data—The new GOME data processor (GDP) version 4: 1. Algorithm description, J.
12 Geophys. Res., 111, D14311, doi:10.1029/2005JD006375, 2006.
- 13 Vlemmix, T., PETERS, A. J. M., Stammes, P., Wang, P., and Levelt, P. F.: Retrieval of
14 tropospheric NO₂ using the MAX-DOAS method combined with relative intensity
15 measurements for aerosol correction, Atmos. Meas. Tech., 3, 1287-1305, doi:
16 10.5194/amt-3-1287-2010, 2010.
- 17 Wagner, T., Dix, B., von Friedeburg, C., Friess, U., Sanghavi, S., Sinreich, R., and Platt, U.:
18 MAX-DOAS O₄ measurements: A new technique to derive information on atmospheric
19 aerosols - Principles and information content, J. Geophys. Res., 109, D22205, doi:
20 10.1029/2004jd004904, 2004.
- 21 Wagner, T., Beirle, S., Brauers, T., Deutschmann, T., Frieß, U., Hak, C., Halla, J. D., Heue, K.
22 P., Junkermann, W., Li, X., Platt, U., and Pundt-Gruber, I.: Inversion of tropospheric
23 profiles of aerosol extinction and HCHO and NO₂ mixing ratios from MAX-DOAS
24 observations in Milano during the summer of 2003 and comparison with independent data
25 sets, Atmos. Meas. Tech., 4, 2685–2715, 2011.
- 26 Wang, T., Nie, W., Gao, J., Xue, L., Gao, X., Wang, X., Qiu, J., Poon, C., Meinardi, S., and
27 Blake, D.: Air quality during the 2008 Beijing Olympics: secondary pollutants and regional

- 1 impact, *Atmos. Chem. Phys.*, 10, 7603-7615, 2010.
- 2 Wang, T., Wang, P., Yu, H., Zhang, X., Zhou, B., Si, F., Wang, S., Bai, W., Zhou, H., and Zhao,
3 H.: Intercomparison of slant column measurements of NO₂ by ground-based MAX-DOAS,
4 *Acta Phys. Sin.*, 62, 054206, doi:10.7498/aps.62.054206, 2013.
- 5 Wang, T., Wang, P., Yu, H., and Sun, L.: Analysis of the characteristics of tropospheric NO₂ in
6 Xianghe based on MAX-DOAS measurement, *Climatic and Environmental Research (in*
7 *Chinese)*, 19 (1): 51–60, 2014.
- 8 Wang, W., Chai, F., Zhang, K., Wang, S., Chen, Y., Wang, X., and Yang, Y.: Study on ambient
9 air quality in Beijing for the summer 2008 Olympic Games, *Air Qual. Atmos. Health*, 1,
10 31-36, 2008.
- 11 Wittrock, F., Oetjen, H., Richter, A., Fietkau, S., Medeke, T., Rozanov, A., and Burrows, J. P.:
12 MAX-DOAS measurements of atmospheric trace gases in Ny-Alesund - Radiative transfer
13 studies and their application, *Atmos. Chem. Phys.*, 4, 955-966, 2004.
- 14 Wu, F., Xie, P., Li, A., Chan, K., Hartl, A., Wang, Y., Si, F., Zeng, Y., Qin, M., and Xu, J.:
15 Observations of SO₂ and NO₂ by mobile DOAS in the Guangzhou Eastern Area during the
16 Asian Games 2010, *Atmos. Meas. Tech.*, 6, 2277–2292, 2013.
- 17 Xia, X., Zong, X., and Sun, L.: Exceptionally active agricultural fire season in mid-eastern
18 China in June 2012 and its impact on atmospheric environment, *J. Geophys. Res. Atmos.*,
19 118, 9889-9900, doi:10.1002/jgrd.50770, 2013.
- 20 Yan, P., Huang, J., and Draxler, R.: The long-term simulation of surface SO₂ and evaluation of
21 contributions from the different emission sources to Beijing city, *Science in China Series D*
22 *(Earth Sciences)*, 48, 196-208, 2005.
- 23 Yan, P., Wang, X., Wang, Z., and Wu, Q.: Analysis of decreases in NO₂ concentrations during
24 Beijing Olympic Games in 2008, *Climatic and Environmental Research (in Chinese)*, 15,
25 609-615, 2010.
- 26 Yang, K., Dickerson, R. R., Carn, S. A., Ge, C., and Wang, J.: First observations of SO₂ from

1 satellite Suomi NPP OMPS: Widespread air pollution events over China, *Geophys. Res.*
2 *Lett.*, 40, 4957-4962, doi:10.1002/grl.50952, 2013.

3 Yu, X., Zhu, B., and Zhang, M.: Seasonal variability of aerosol optical properties over Beijing,
4 *Atmos. Environ.*, 43, 4095-4101, 2009.

5 Yu, H., Wang, P., Zong, X., Li, X., and Lü, D.: Change of NO₂ column density over Beijing
6 from satellite measurement during the Beijing 2008 Olympic Games, *Chinese Science*
7 *Bulletin*, 55, 308-313, 2010.

8 Zhao, B., Wang, P., Ma, J. Z., Zhu, S., Pozzer, A., and Li, W.: A high-resolution emission
9 inventory of primary pollutants for the Huabei region, China, *Atmos. Chem. Phys.*, 12,
10 481-501, 2012.

11

1 Table 1: Settings used for the SO₂ and O₄ DOAS analysis.

Parameter	Data source	Fitting interval (nm)	
		338-370 (O ₄)	305-317.5(SO ₂)
NO ₂	Vandaele et al. (1998) 220K, 294K	x	x(only 294K)
SO ₂	Vandaele et al. (1994) 294K		x
O ₃	Bogumil et al. (2003) 223K, 243K	x(only 223K)	x
O ₄	Hermans et al. (2003) 296K	x	
BrO	Fleischmann et al. (2004) 223K	x	
H ₂ CO	Meller and Moortgat (2000) 293K	x	
Ring	Chance and Spurr (1997)	x	x
Polynomial degree		5	5

2

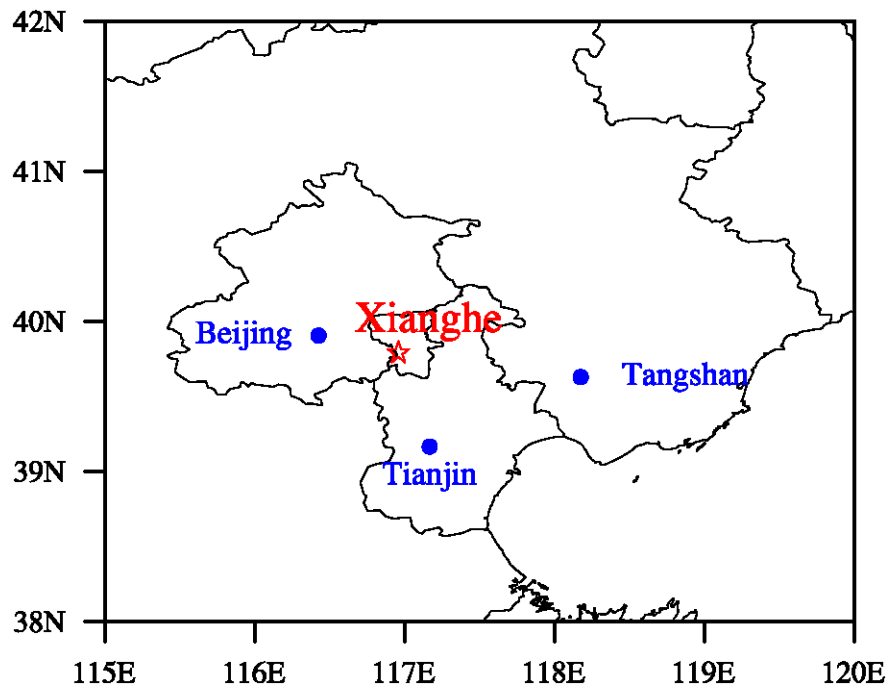
3

1 Table 2: Error budget of retrieved SO₂ concentration (0-200m) and VCD.

Uncertainty (%)	Concentration (0-200m)	VCD
Smoothing + noise errors	16	11
Uncertainty related to aerosols	16	5
Uncertainty related to the a priori	8	19
Uncertainty on SO ₂ cross section	5	5
Total uncertainty	24	23

2

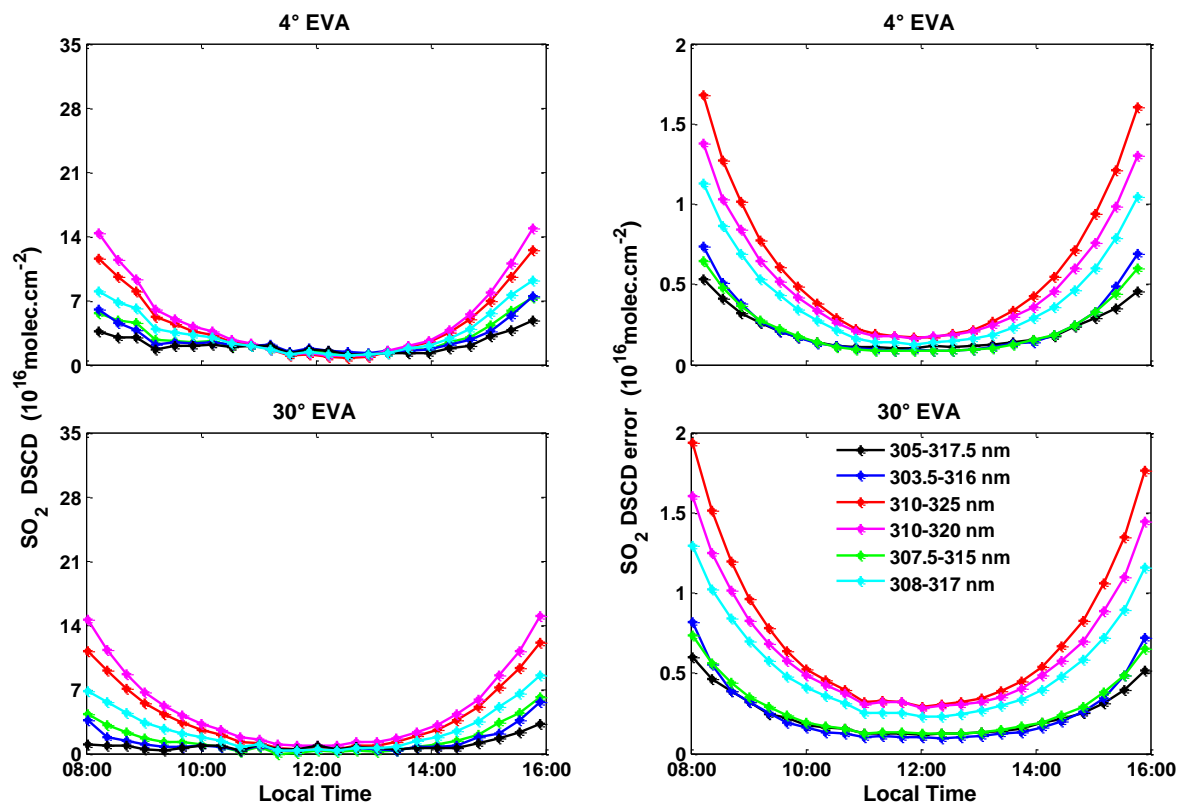
3



1

2 Figure 1: Location of the Xianghe Observatory and major neighborhood cities.

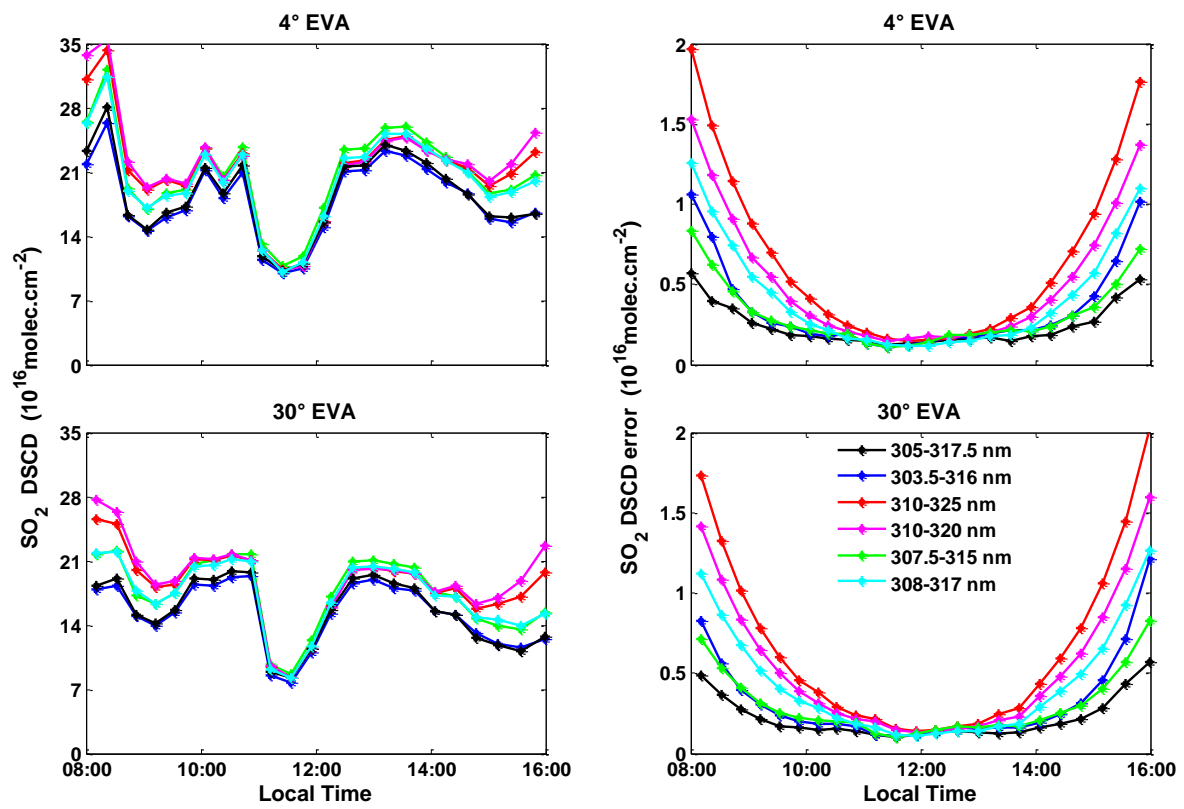
3



1

2 Figure 2: SO₂ DSCDs (1st column) and corresponding fitting uncertainties (2nd column) retrieved at 4°
 3 (upper plots), 30° (lower plots) elevation for different wavelength intervals on 1st October 2011.

4



1

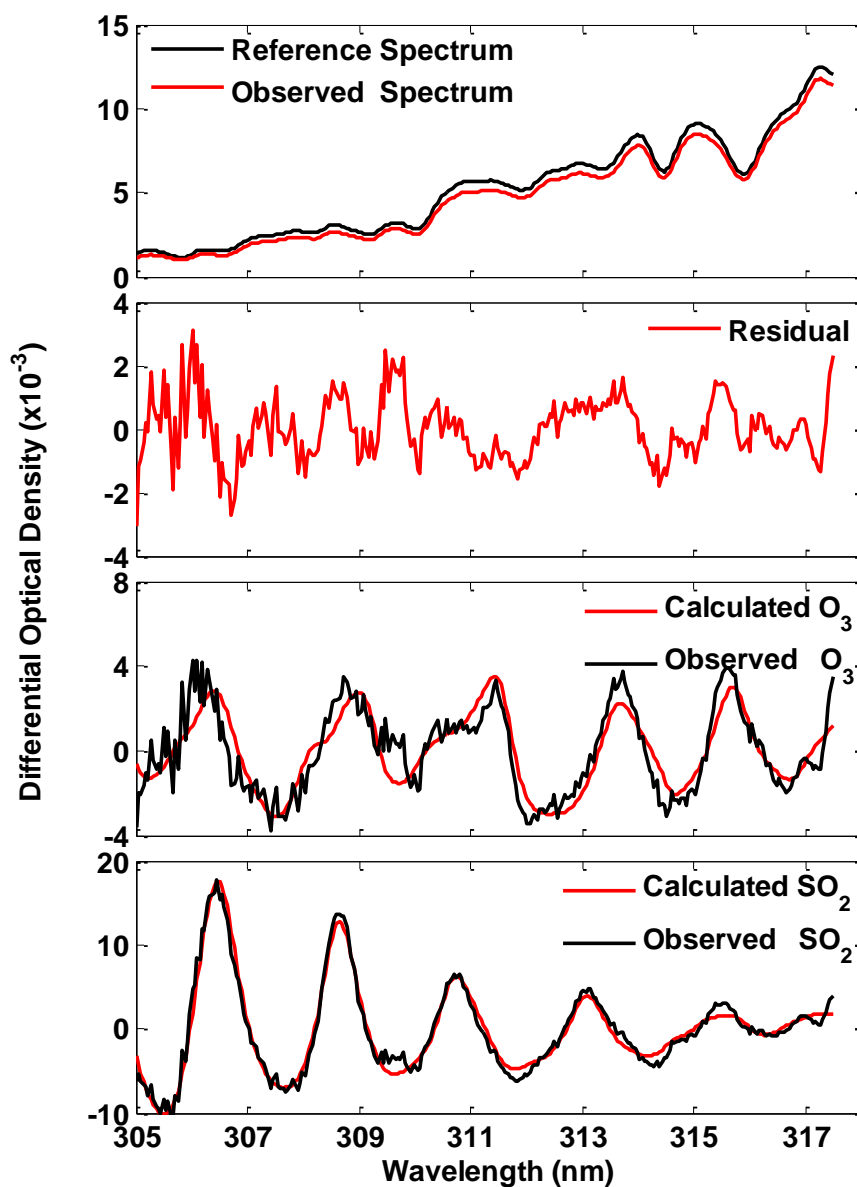
2

Figure 3: Same as Figure 2, but for 4th October, 2011.

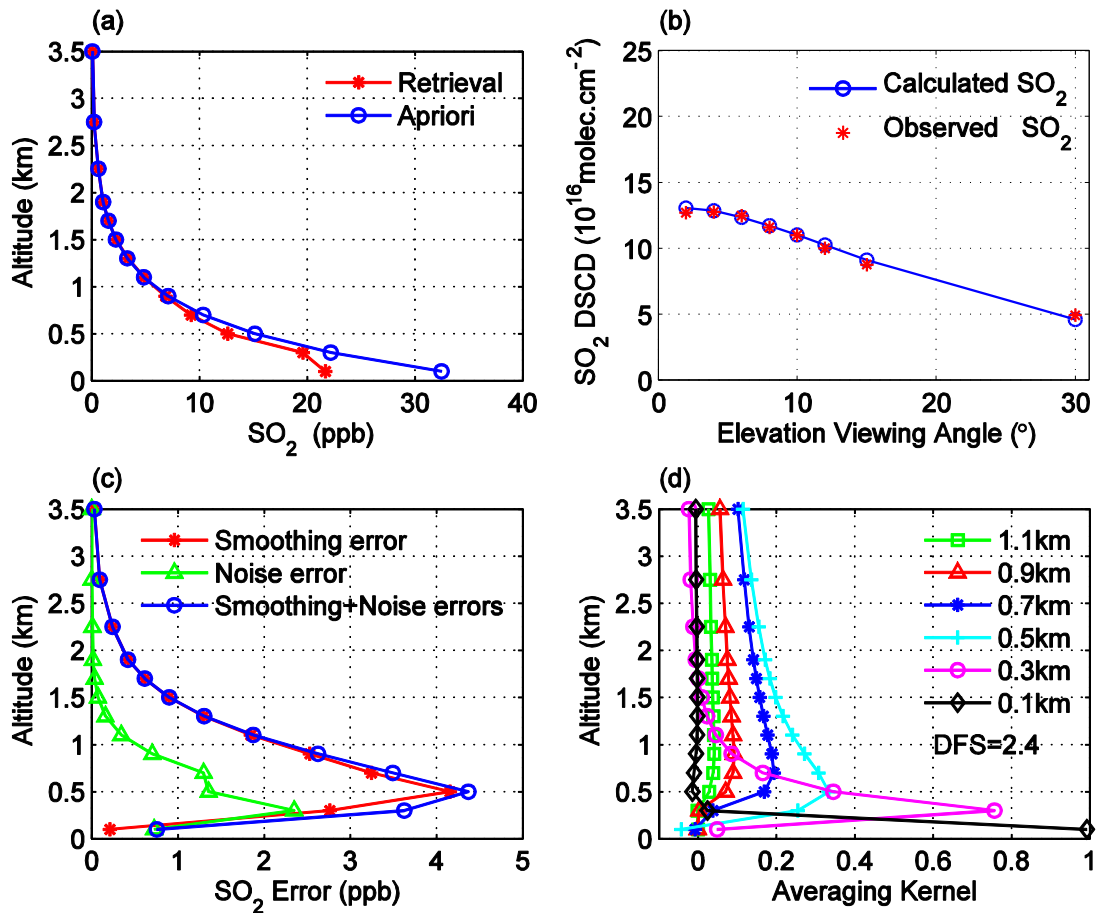
3

4

5



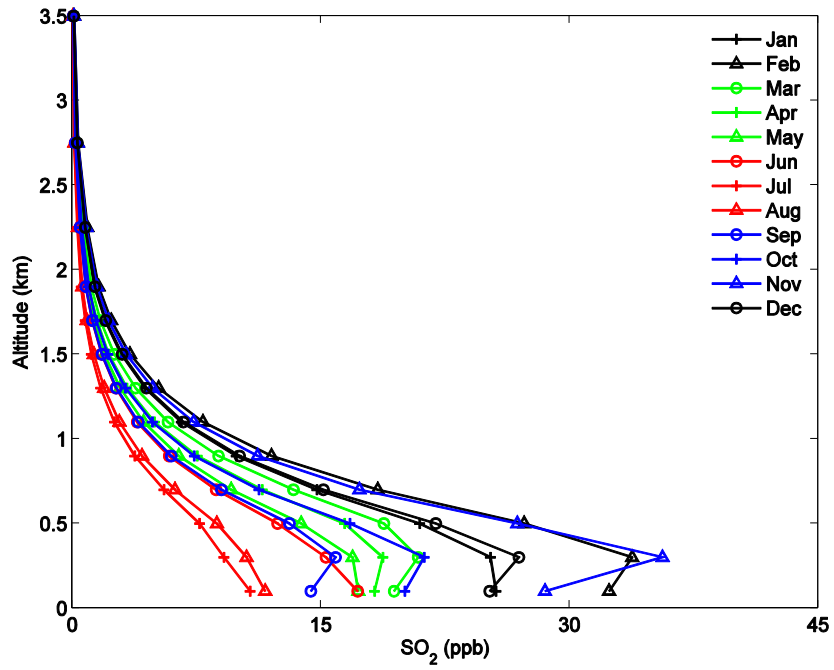
1
 2 Figure 4: Example of DOAS fit result for SO₂. It corresponds to 29 September 2010 at ~11:20
 3 LT. SZA and EVA values are 43° and 30°, respectively.
 4



1

2 Figure 5: Example of SO₂ vertical profile retrieval from MAX-DOAS measurements at
 3 Xianghe (29 September, 2010 at 10:15 LT). (a) a priori (blue) and retrieved profile (red); (b)
 4 observed (red) and calculated (blue) DSCD (c) smoothing error (red), noise error (green) and
 5 sum of these two (blue); (d) averaging kernels.

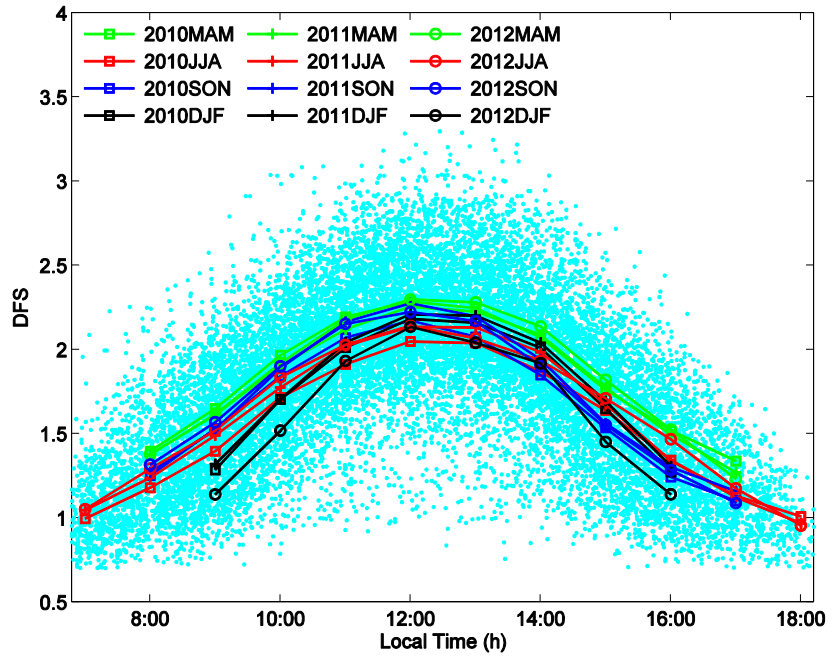
6



1

2 Figure 6: Monthly-averaged SO₂ concentration vertical profiles for the March 2010 -
 3 February 2013 period.

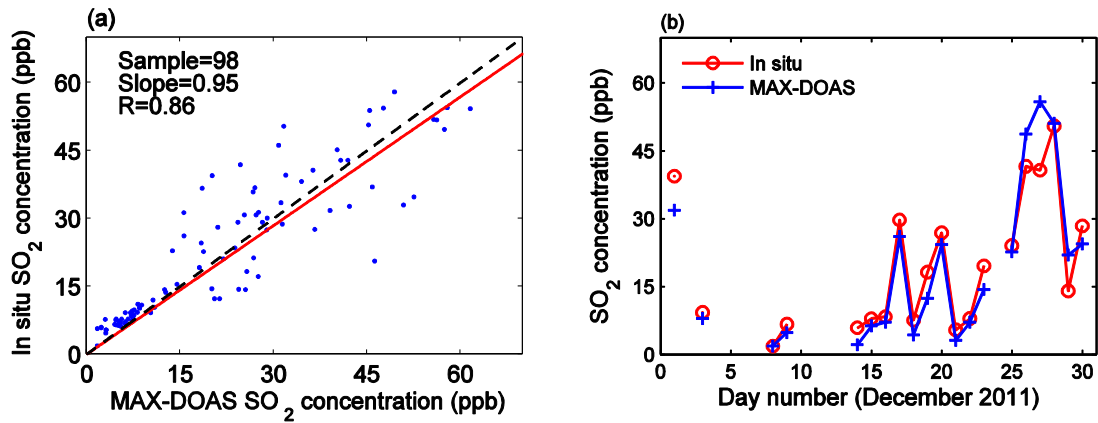
4



1

2 Figure 7: Seasonally-averaged DFS diurnal cycles corresponding to the SO₂ profile retrievals.

3



1

2 Figure 8: (a) Scatter plot of in situ SO₂ surface concentrations (0-200m layer) against

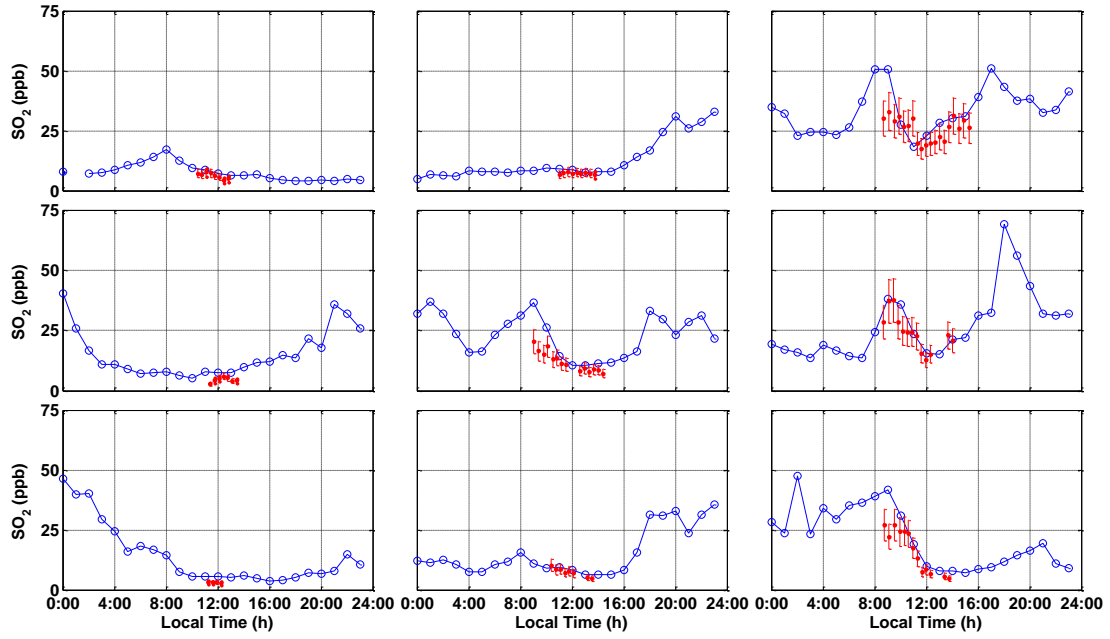
3 MAX-DOAS data for December 2011 (hourly-averaged concentrations). The red line denotes

4 the linear least-squares fit to the data. (b) Temporal evolution of daily averaged MAX-DOAS

5 and in situ SO₂ concentrations during December 2011. Gaps in the data series are due to

6 missing MAX-DOAS measurements.

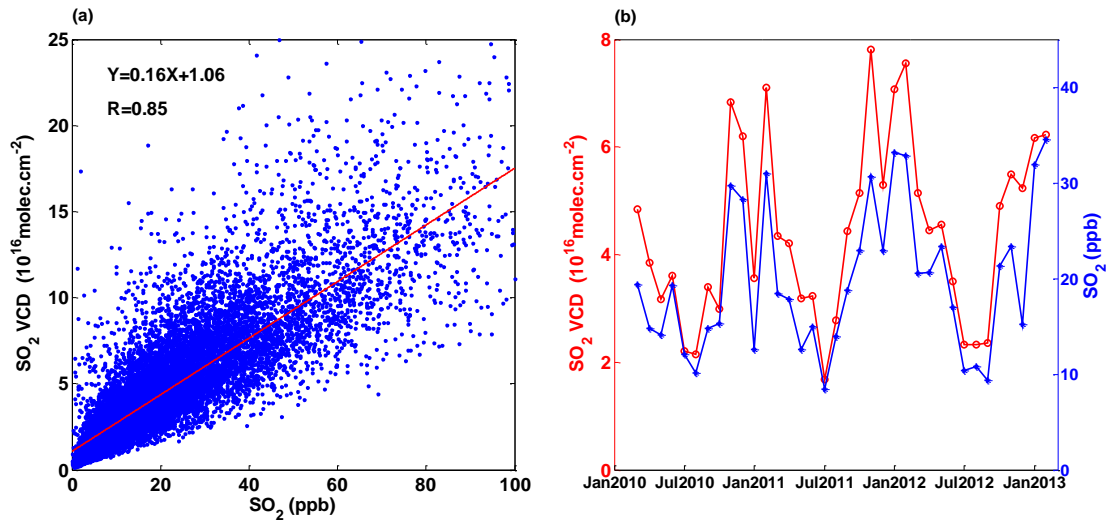
7



1

2 Figure 9: Comparison between in situ (blue, hourly means) and MAX-DOAS SO₂ surface
 3 concentrations (red, each point represents the retrieval from one scan) for the December 15-23,
 4 2011 period (upper plots are for December 15-17, middle plots are for December 18-20, lower
 5 plots are for December 21-23).

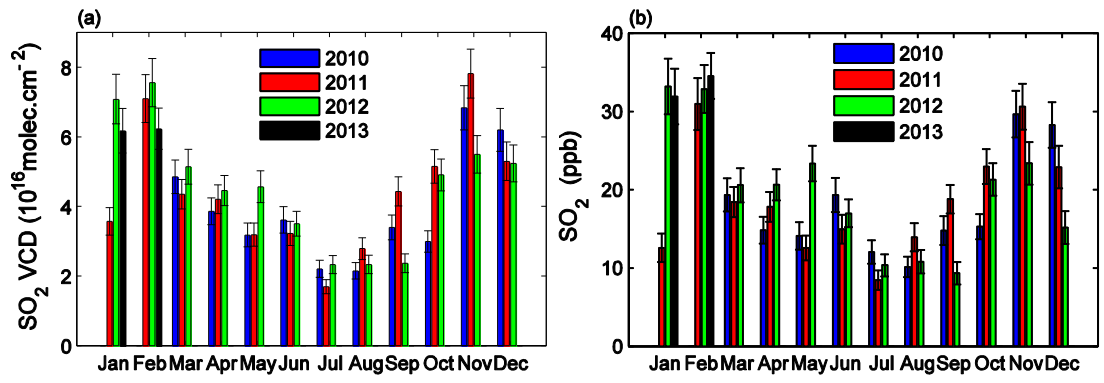
6



1

2 Figure 10: (a) Scatter plot of SO₂ VCD against surface concentration. The red line represents
 3 the linear least-squares fit to the data. (b) Temporal evolutions of monthly mean VCD and
 4 concentration from March 2010 to February 2013.

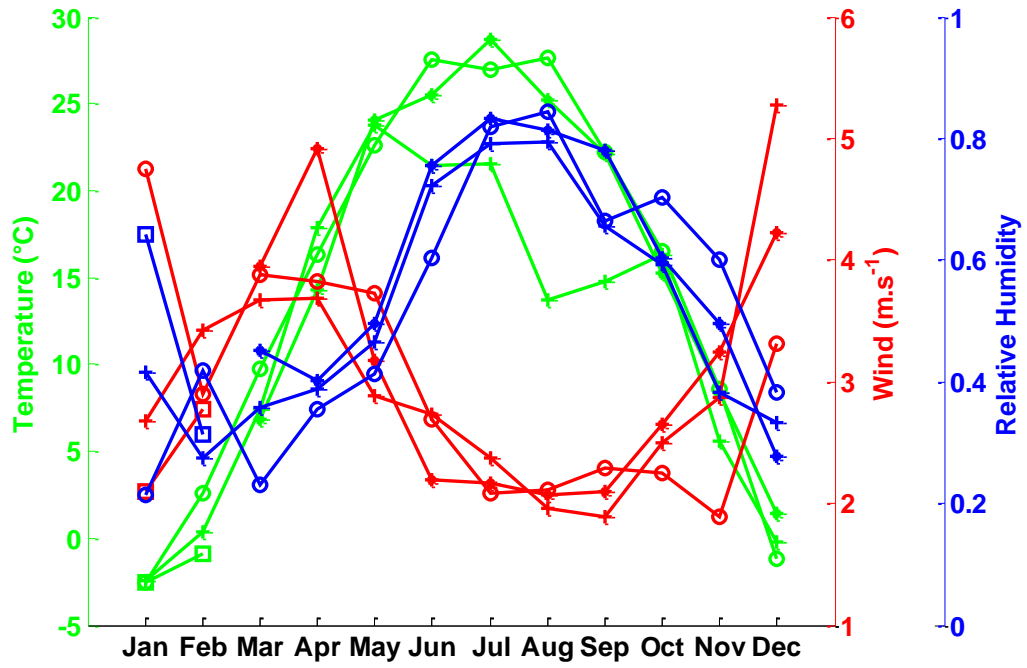
5



1

2 Figure 11: Monthly mean SO₂ VCD (a) and surface concentration (b) for the March 2010 -
 3 February 2013 period.

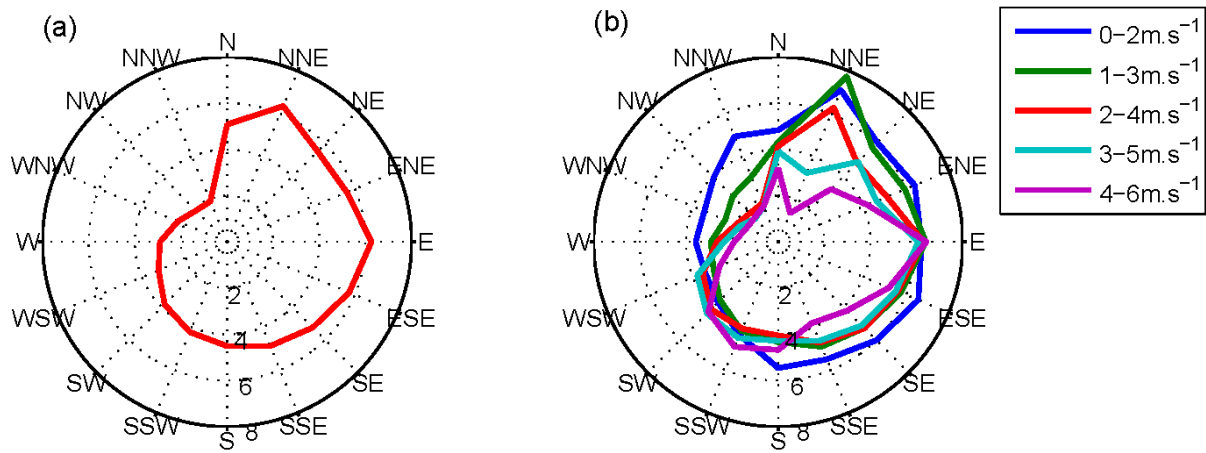
4



1

2 Figure 12: Seasonal cycles (monthly means) of temperature, humidity, and wind speed in
 3 2010 (marker: star), 2011 (plus), 2012 (circle), and 2013 (square).

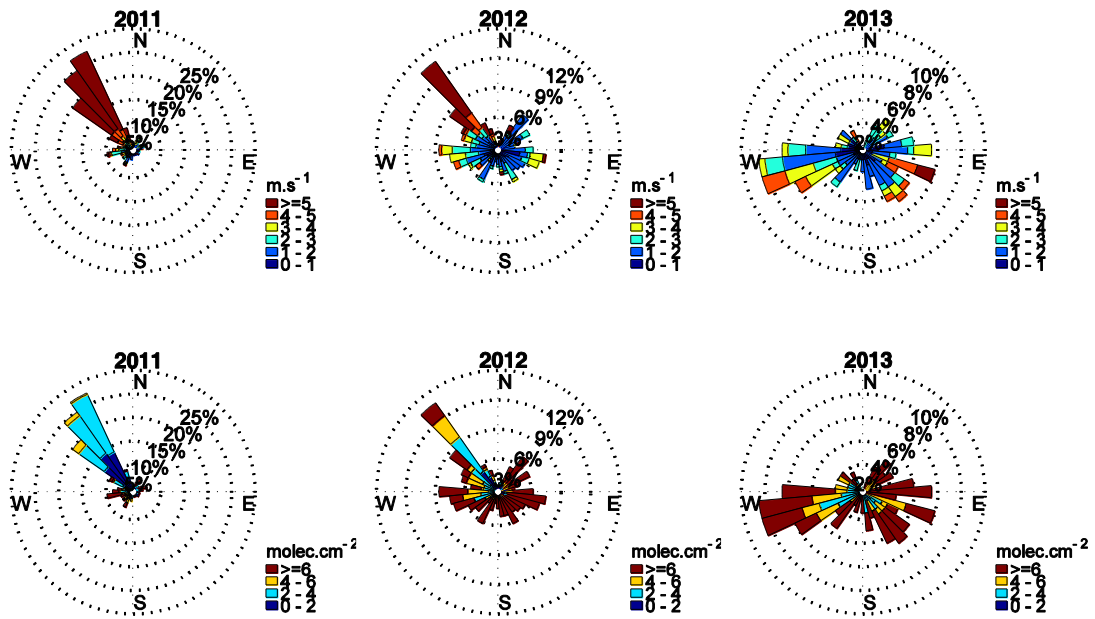
4



1

2 Figure 13: (a) Wind rose showing the SO₂ VCD (10^{16} molec.cm⁻²) as a function of the wind
 3 direction (average for all wind speed). (b) Dependence of SO₂ VCD (10^{16} molec.cm⁻²) on
 4 wind direction for different wind speeds.

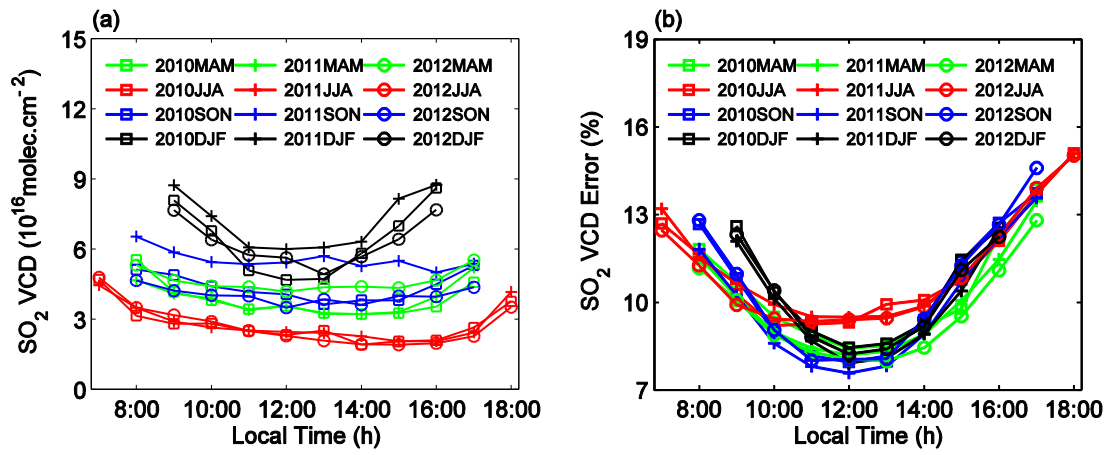
5



1

2 Figure 14: Wind rose for wind speed (1st row; m.s^{-1}) and SO_2 VCD (2nd row; $10^{16} \text{ molec.cm}^{-2}$)
 3 for January 2011 (1st column), 2012 (2nd column), and 2013 (3rd column).

4

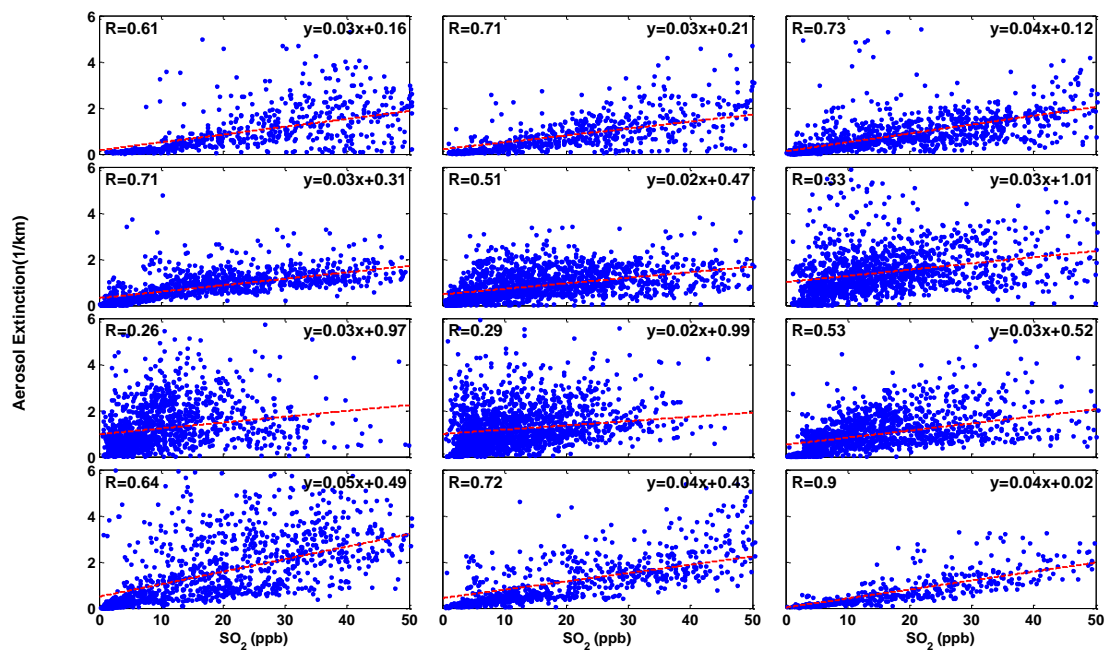


1

2 Figure 15: (a) Seasonally-averaged SO₂ VCD diurnal cycles, and (b) corresponding errors.

3 Data points represent hourly means.

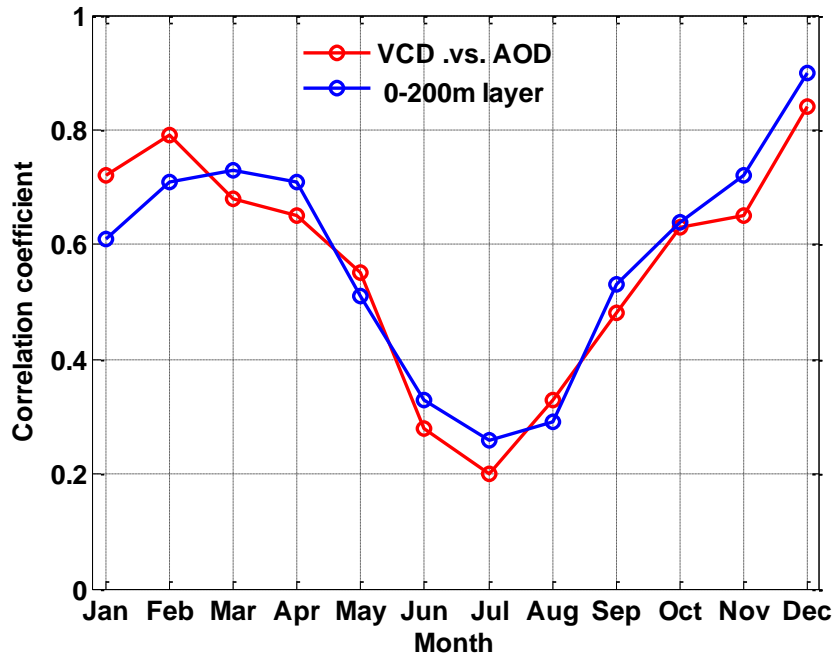
4



1

2 Figure 16: Scatter plots of aerosol extinction coefficient versus SO₂ concentration in the
 3 0-200m layer for months 1-12 of the March 2010 – February 2013 period (first row is for JFM,
 4 second row for AMJ, third row for JAS, and fourth plots for OND). The data points
 5 correspond to the different MAX-DOAS scans. The red line denotes the linear least-squares
 6 fit to the data.

7



1
2
3
4
5

Figure 17: Seasonal variation of the correlation coefficient between SO₂ and aerosols over the March 2010-February 2013 period. The red curve corresponds to VCD versus AOD and the blue curve to SO₂ concentration versus aerosol extinction coefficient in the 0-200m layer.